Geophysical Research Letters

Supporting Information for

Greenland subglacial discharge as a driver of hotspots of increasing coastal chlorophyll since the early 2000s

Hilde Oliver[1], Donald Slater[2,3], Dustin Carroll[4,5], Michael Wood[4], Mathieu Morlighem[6], Mark J. Hopwood[7]

1. Department of Applied Ocean Physics and Engineering, Woods Hole Oceanographic Institution, MA, USA
2. School of Geosciences, University of Edinburgh, UK
3. School of Geography and Sustainable Development, University of St Andrews, UK
4. Moss Landing Marine Laboratories, San José State University, Moss Landing, CA, USA
5. Jet Propulsion Laboratory, California Institute of Technology, Pasadena, CA, USA
6. Department of Earth Sciences, Dartmouth College, Hanover, NH, USA
7. Department of Ocean Science and Engineering, Southern University of Science and Technology, Shenzhen, China

Contents of this file

Introduction

Text S1 describes the compilation of the shelf nitrate profiles, Text S2 further describes the buoyant plume model, Text S3 provides information on the ECCO mixed layer depths used for comparison with satellite Chl, and Text S4 describes the comparison between modeled and observed/derived nitrate fluxes (with comparisons shown in Table S1).

Figure S1 is the same as Fig. 2 in the main text, except with uncertainty shading arising from varying the plume width instead of subglacial discharge; Figure S2 shows the largest modeled upwelling systems; Figure S3 shows how Chl relationships with discharge and nitrate flux anomaly change with increasing mask size; Figure S4 shows the power law relationship between predicted nitrate flux and subglacial discharge rate, grounding line nitrate concentration, and grounding line depth; Figure S5 shows the ECCO mixed layer depths within individual upwelling systems. Figure S6 illustrates examples of initial nitrate initial profiles in two sectors.

Text S1.

To determine the best-available nitrate profiles for the plume model, we compiled a spatially-extensive dataset of available nitrate profiles from the Greenland shelf (1895–2020). Nutrient data were compiled from pre-existing compilations and recent cruise data that passed quality controls as per (Codispoti et al., 2013). In addition to datasets available from the Bedford Institute of Oceanography (Devine et al., 2014), Greenland Ecosystem Monitoring Project (GEM), GLODAPv2 (Olsen et al., 2020), GEOTRACES (Schlitzer et al., 2018), and the previously compiled pan-Arctic compilation (Codispoti et al., 2013); additional recent temperature, salinity, pressure, and nitrate cruise data was added (Achterberg et al., 2018; Cape et al., 2019; Graeve et al., 2019; Graeve & Ludwichowski, 2017; Hendry, 2018; Kanna et al., 2018; Lund-Hansen et al., 2018; Meire et al., 2017; Paulsen et al., 2017; Zielinski et al., 2013) (Fig. 1). Many of these profiles are located near the SW or NE sectors of the shelf; fewer nitrate profiles are available in Baffin Bay or SE Greenland. To generate profiles, we first computed 10 m vertically-binned statistical means and then applied a moving average filter. As the data become sparser with depth, we employed an expanding filter window: over the top 150 m, a 100 m moving window was used, with a 250 m window used below this depth. Below 600 m, we use the 600 m value, as this is defined as the shelfbreak depth.

When applying the smoothed profiles to the plume model, we assumed that the nitrate concentration in the fjord was equal to the nitrate concentration in the shelf profile at the sill depth (Fig. S6). Unlike nitrate data, which were collected from the shelf, we did not modify temperature and salinity profiles below the sill depth, as nearly all the temperature and salinity profiles were collected inside the fjords. Because the nutrient profiles are relatively uniform at depth, modifying the sill depth has little effect on nitrate entrainment calculated by the plume model; varying the sill depth by ±20% resulted in a +4%/-8% change in the summed pan-Greenland modeled nitrate flux anomaly.

While nitrate concentrations may undergo some transformation during transit from the shelf to glacier termini, case studies at Sermilik (Cape et al., 2019), Nioghalvfjerdsbrae ("79 North") (Krisch et al., 2021), and Bowdoin (Kanna et al., 2018) suggest that these changes are minor or statistically insignificant compared to near-glacier mixing. We use a static nitrate profile throughout the meltwater season because there is not likely to be strong seasonal variability in nitrate below the euphotic zone (<40 m) and the nitrate profiles used were generally collected after the annual spring bloom when surface nitrate is depleted (except in SE Greenland where nitrate is not limiting on the shelf).

Text S2.

The buoyant plume model used in this study is a line plume model that is identical to that considered in Jenkins (2011), Slater et al. (2016) and Slater et al. (2022). For a precise description of the model equations and physics we refer the reading to the supplement of Slater et al. (2016). The plume model computes in-plume profiles of temperature, salinity, velocity, volume flux, and nitrate concentration from the grounding line to neutral buoyancy depth, which is the depth at which the plume stops rising and flows away from the glacier. Note that the neutral buoyancy depth is distinct from the maximum plume height, which is the depth to which the plume's inertia can drive the kinetic overshooting of the neutral buoyancy depth.

The inclusion of nitrate in the buoyant plume model required an additional equation, which can be written as:

$$\frac{\mathrm{d}}{\mathrm{dz}}(\mathrm{buNO_3}) = \alpha\mathrm{uNO_{3s}} \tag{1}$$

where b is the plume width, u is the plume velocity, NO3 is the concentration of nitrate in the plume, α is the plume entrainment constant (set to 0.1) and NO_{3s} is the concentration of nitrate in the ambient fjord waters. This equation states that the vertical flux of nitrate in the plume changes due to the entrainment of nutrients into the plume from the fjord. We assume there is a negligible flux of nitrate to the ocean through the ice-ocean boundary, and therefore we do not include a submarine melt component in the equation.

Model inputs include grounding line depth, subglacial discharge flux, and vertical profiles of temperature, salinity, and nitrate. In the absence of sufficient data to resolve time variability, constant temperature, salinity, and nitrate profiles are used. When exploring the variability in nitrate fluxes between glaciers (Section 3.1 of the Results), we apply applied 3 different rates of of subglacial discharge: (1) 2010-2019 JJA mean, (2) maximum monthly discharge in any month during 2010-2019, and (3) minimum monthly discharge in any month during 2010-2010. When computing NFA for comparison with the satellite Chl product (Section 3.2 of the results), we calculate NFA using the mean subglacial discharge for each period (early, late, and full summer, following the definitions from the Main Text), for each year (2003-2018).

Text S3.

To compare satellite Chl with mixed layer depth, we use monthly output from the Estimating the Circulation and Climate of the Ocean (ECCO) LLC 270 global-ocean and sea-ice data synthesis (Zhang et al., 2018), which extends from 1992–2017. Physical observations are assimilated using the adjoint method, which minimizes a weighted least squares sum of model-data misfit to optimize initial conditions, time-varying surface-ocean boundary conditions, and time-invariant, three-dimensional mixing coefficients for along-isopycnal, cross-isopycnal, and isopycnal thickness diffusivity. While there is uncertainty and potential model error associated with the ECCO LLC 270 representation of mixed layer depth, the use of the data-constrained model permits a complete analysis of seasonal mixed layer depth variability in our regions of interest. Within the regional masks shown in Fig. 5, we calculate the mean monthly mixed layer depth (de Boyer Montégut, 2004). Seasonal June–Sept mixed layer depths were then calculated as the average of these monthly means for 2003–2017 for comparison with Chl. We used the entire 1992–2017 product for the mixed layer depth climatology (**Fig. S5**).

Text S4.

We compare modeled plume nitrate, nitrate anomaly, and nitrate fluxes with observation-based estimates from five well-sampled Greenlandic fjord systems: Sermilik

Fjord (Helheim glacier (Cape et al., 2019)), Bowdoin Fjord (Bowdoin glacier (Kanna et al., 2018)), Godthåbsfjord (KNS (Meire et al., 2017)), Ilulissat Icefjord (Jakobshavn Isbræ (Cape et al., 2019)), and Nioghalvfjerd Fjord ("79° North Glacier" (Krisch et al., 2021)). Summertime (July or August) transects along the plumes within these fjords in prior work have provided sufficient salinity, temperature, and nutrient concentration data to obtain a snapshot of the nitrate anomalies close to marine-terminating glaciers, except Ilulissat Icefjord, where typical water mass endmember nutrient constituents were assumed (Cape et al., 2019). In the case of Sermilik and Ilulissat Icefjord, nitrate upwelling was estimated via assumed dilution factors for subglacial cischarge, a method that is similar in spirit to using a buoyant plume model (Cape et al., 2019). The upwelling comparisons with Cape et al., (2019) are thus not true model-data comparisons, as we are comparing two similar model estimates. For Bowdoin, an estimate of the nitrate flux was derived from estimates of the down-fjord plume velocity and nitrate content as per Kanna et al., (2018). For KNS, estimates of the nitrate anomaly and NFA are derived herein from scaling to prior estimates for upwelling of silicic acid in KNS (Meire et al., 2016), and for Nioghalvfjerdsbrae, from volume fluxes and concentrations emerging from the Nioghalvfjerdsbrae floating ice tongue as per Ref Krisch et al., (2021).

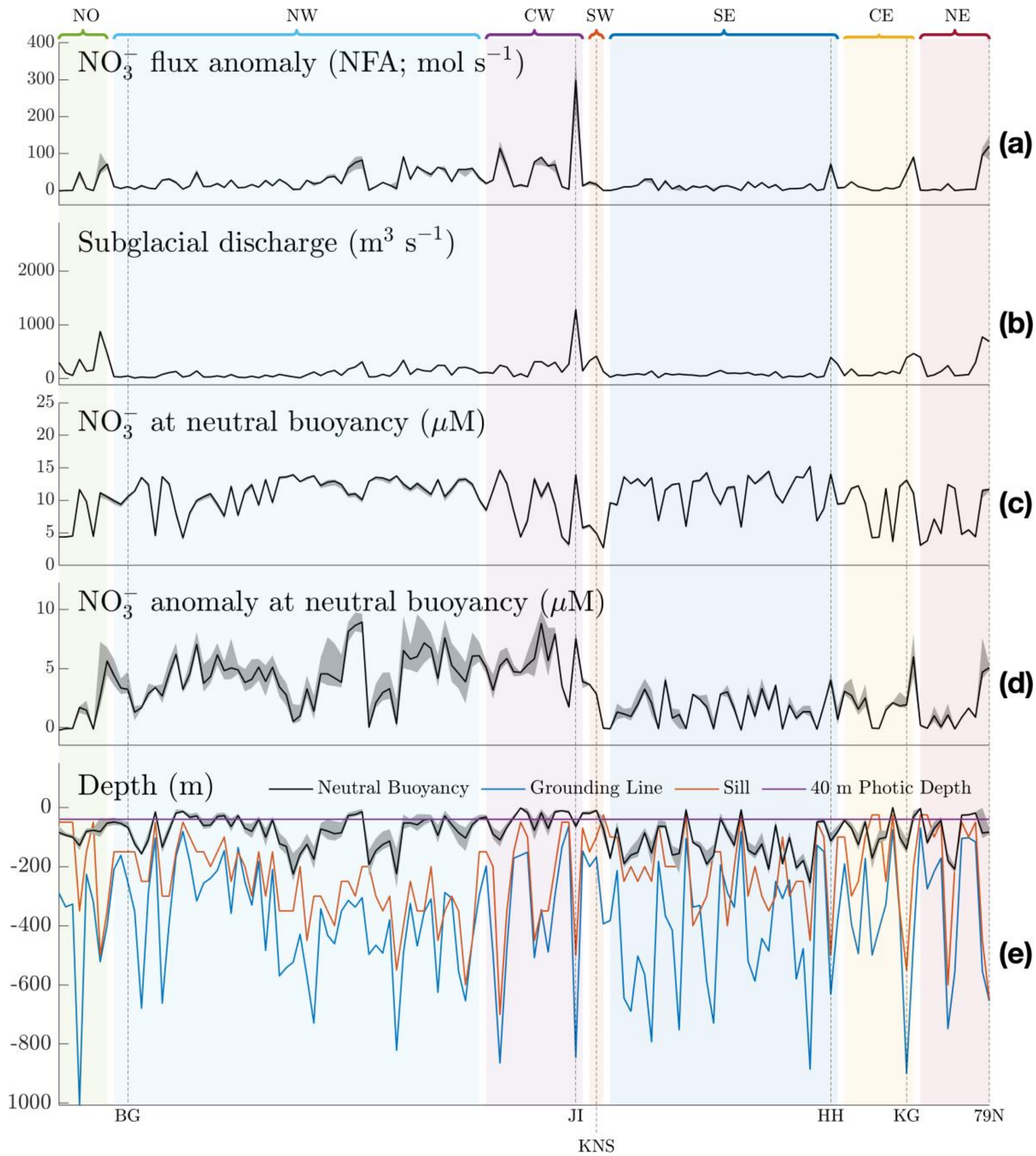

Figure S1. Modeled pan-Greenland nitrate fluxes, as in Figure 2 in the main text, except with uncertainty shading arising from the plume width instead of subglacial discharge variability. Model results for a 200-m wide line plume are plotted in black; gray shading shows spread when using a 100 m- or 300 m-wide line plume. (a) The modeled NFA; (b) mean summer subglacial discharge rates; (c) modeled nitrate at neutral buoyancy; (d) nitrate anomaly at neutral buoyancy; (e) modeled neutral buoyancy depths, with grounding line depths, sill depths, and an estimated 40 m photic depth. Glaciers are ordered counterclockwise around Greenland, starting from the north (left). Bowdoin Glacier (BG), Jakobshavn Isbræ (JI), Kangiata Nunata Sermia (KNS) glacier, Helheim

Glacier (HH), Kangerlussuaq Glacier (KG) and Nioghalvfjerdsbrae (79°N) glacier are highlighted by the dashed lines.

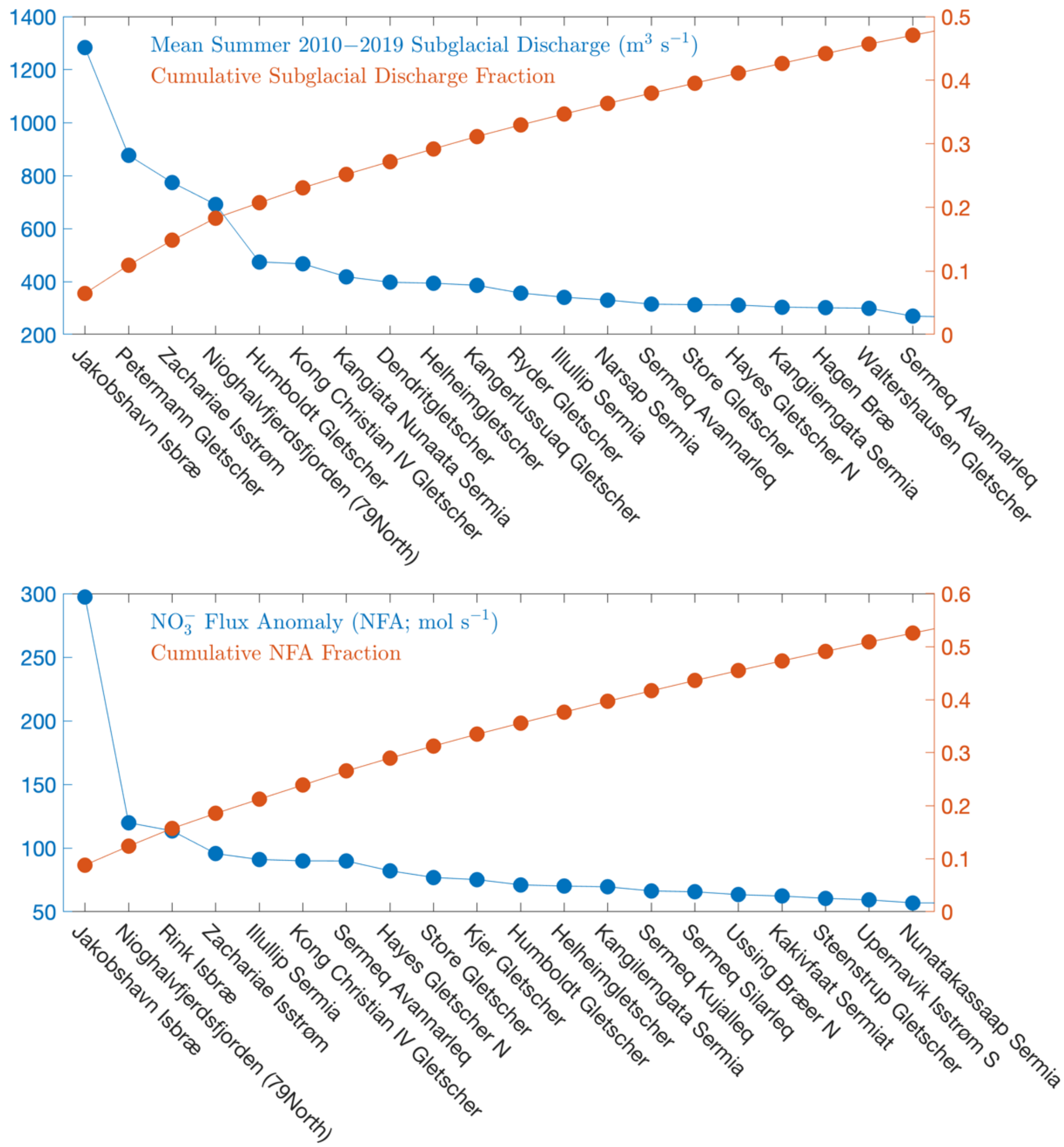

Figure S2. Most significant glaciers as measured by subglacial discharge and nitrate flux. Glaciers are ordered by subglacial discharge (**top**) and NFA (**bottom**). Values are mean 2010–2019 summer estimates, and assuming a 200-m plume width.

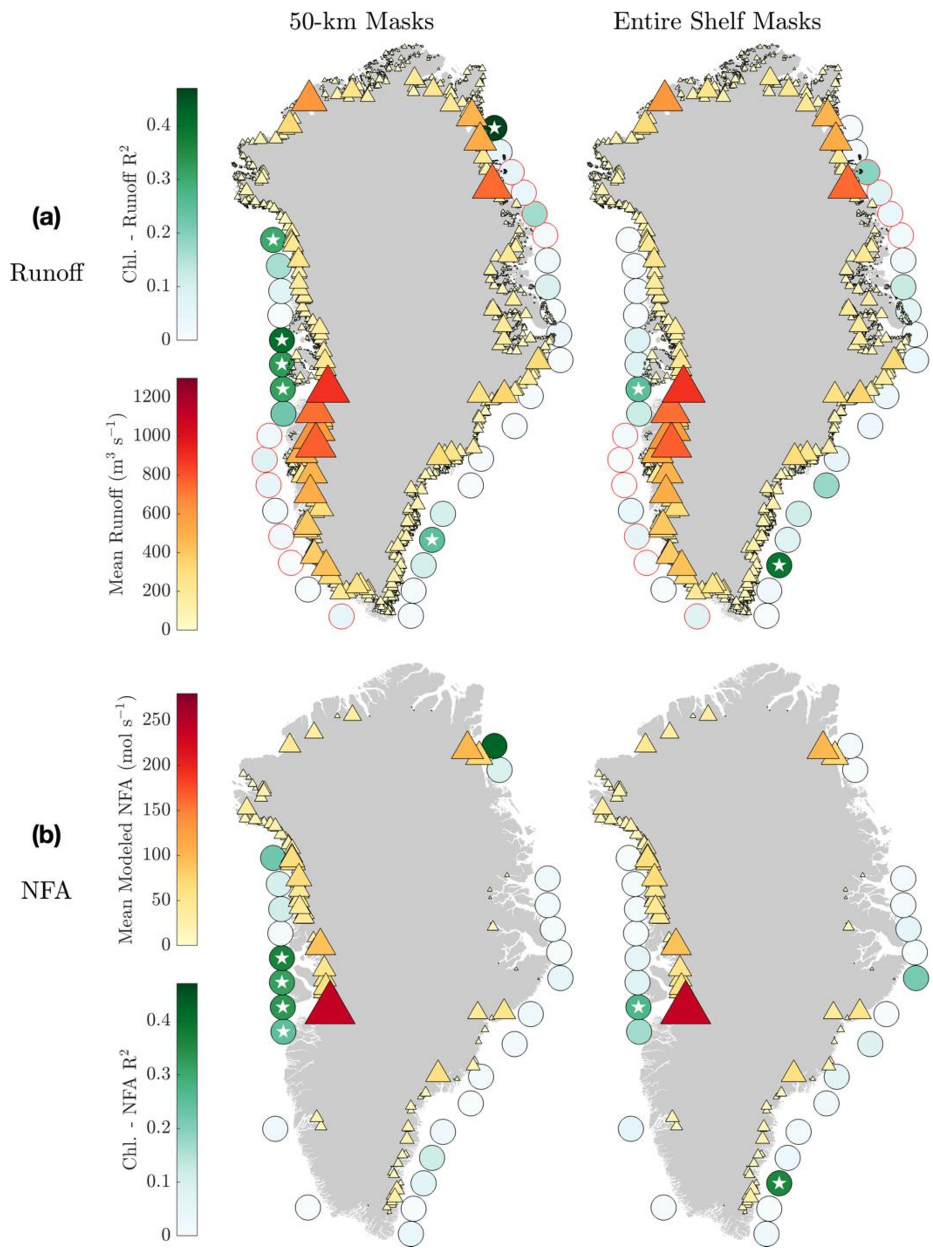

Figure S3. Interannual Chl variability relative to (**a**) runoff and (**b**) modeled NFA, for 50-km and shelf-wide masks. The size and color of the triangles indicates the magnitude of runoff from glaciers (top row) and modeled NFA from marine-terminating glaciers (bottom row). Green circles indicate the proportion of interannual Chl variability in each latitude band that is explainable by interannual variability in runoff or NFA. Red outlines in the top row indicate latitude bands having no marine-terminating glaciers, while white stars indicate statistically significant relationships.

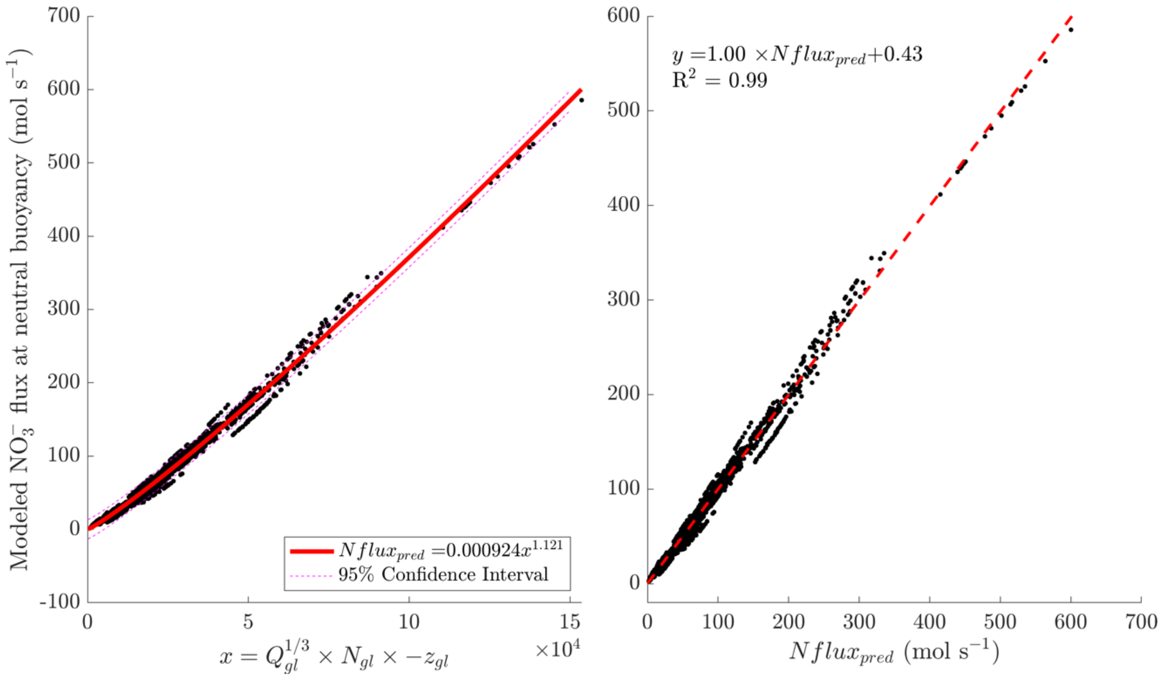

Figure S4. Modeled seasonal (June–September) annual (2003–2018) estimates of nitrate fluxes ($Nflux_{pred}$) at neutral buoyancy vs. power law estimates as a function of subglacial discharge (Q_{gl}), grounding line nitrate concentration (N_{gl}), and grounding line depth (z_{gl}).

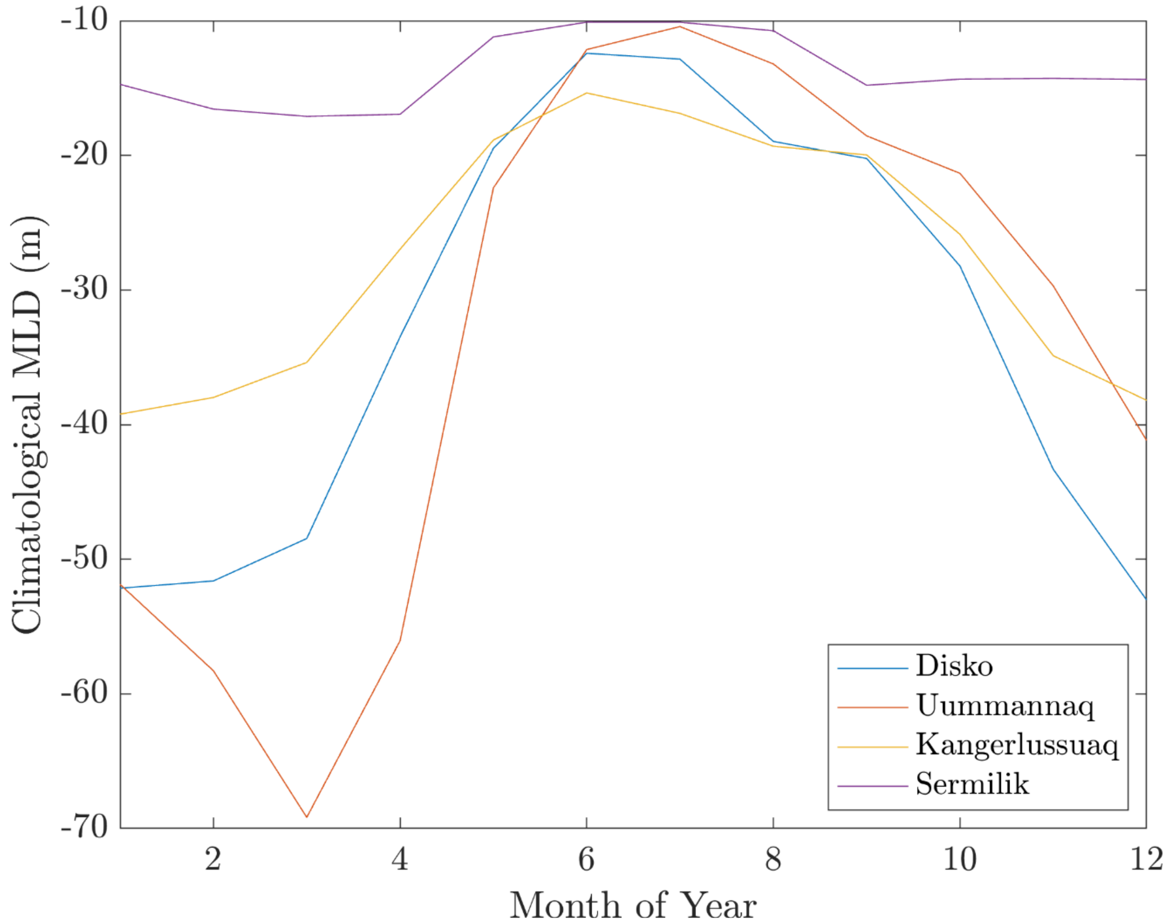

Figure S5. Monthly climatological mixed layer depth (Zhang et al., 2018) (mixed layer criterion from de Boyer Montégut (2004)) within the individual upwelling systems shown in Figure 4.

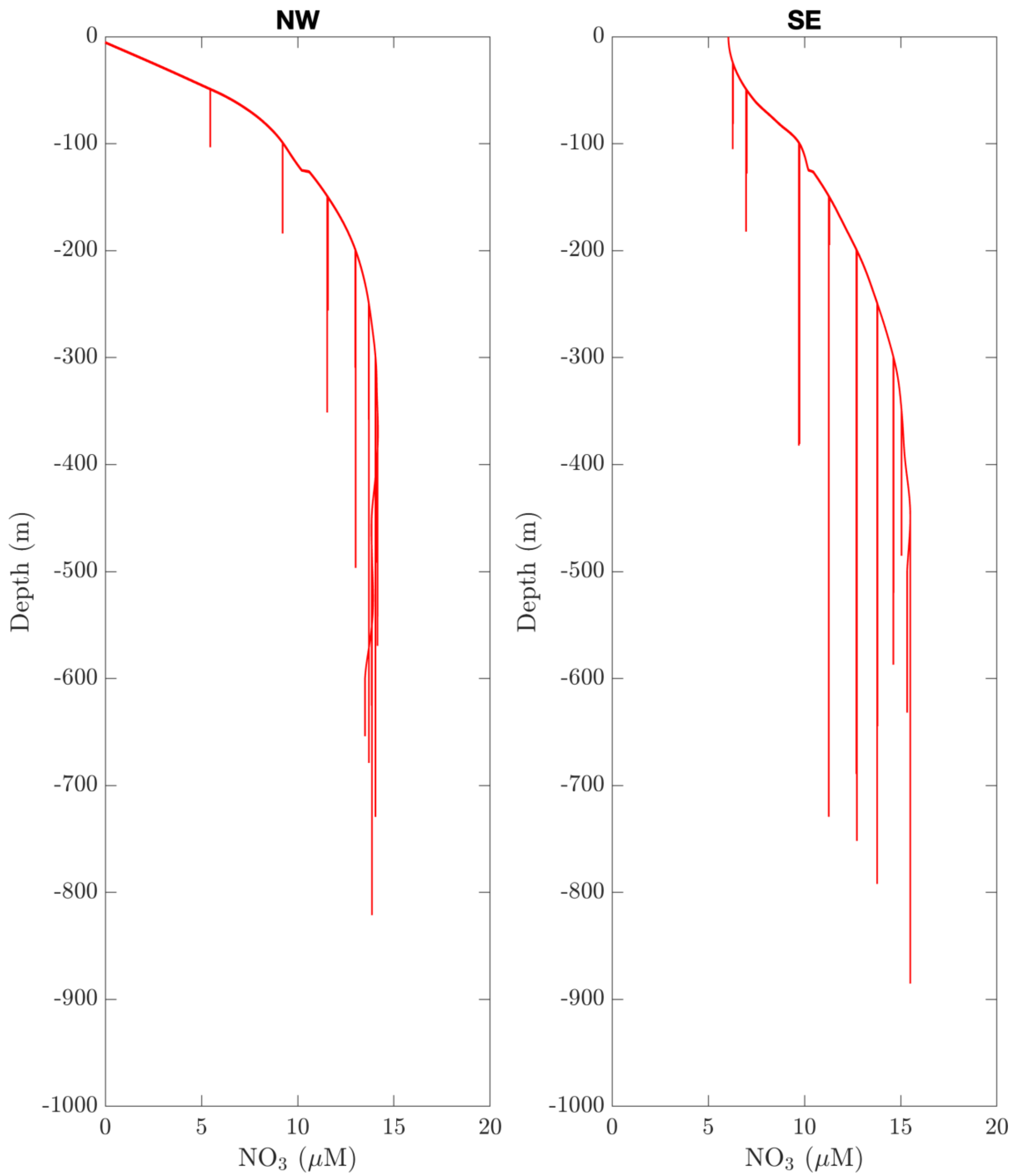

Figure S6. Nitrate profiles for the model, for the northwest (NW), and southeast (SE) sectors. Profiles are considered uniform below each sill depth.

Table S1. Model-data comparisons. Estimates derived from observations at various fjord systems around Greenland compared to plume model values, using the minimum and maximum seasonal subglacial discharge estimates from 2010 – 2019.

System	Estimate	Units	Mean	Modeled
79° NG	N outflow	μM		11.2 – 12.4
	N anomaly	μM	2.4±2.1 [a]	2.8 – 4.6
	N flux	mol s^{-1}		277 – 392
	NFA	mol s^{-1}	109±100 [a]	25 – 192
Sermilik Fjord	N outflow	μM	12±0.8 [b]	13.7 – 14.5
	N anomaly	μM	4 [b]	2.9 – 4.6
	N flux	mol s^{-1}	157±36 [b]	153 – 322
	NFA	mol s^{-1}		31 – 109
KNS	N outflow	μM	10 – 12 [c]	4.9 – 5.5
	N anomaly	μM	2 – 7 [c]	2.6 – 2.8
	N flux	mol s^{-1}	2 – 15 [c]	17 – 40
	NFA	mol s^{-1}		8 – 24
Bowdoin Fjord	N outflow	μM	12.3±0.6 [d]	9.9 – 11.1
	N anomaly	μM	7.9±0.4 [d]	2.1 – 5.4
	N flux	mol s^{-1}	21 [d]	18 – 48
	NFA	mol s^{-1}		3 – 26
Ilulissat Icefjord	N outflow	μM		13.5 – 14.6
	N anomaly	μM		5.2 – 8.2
	N flux	mol s^{-1}	368±110 [e]	349 – 729
	NFA	mol s^{-1}		123 – 445

a. Calculated from Krisch et al., 2021, August sampling
b. Derived in Cape et al., 2019, August sampling
c. Calculated from Meire et al., 2017, August sampling
d. Calculated from Kanna et al., 2018, July sampling
e. Derived in Cape et al., 2019, N flux converted from 40.1±12 Gg N yr^{-1}, nutrient endmembers from Azetsu-Scott et al., 2012, September–October sampling